Advances in Optics and Photonics

Ultrafast laser processing of materials: a review

KATHERINE C. PHILLIPS,[1] HEMI H. GANDHI,[1] ERIC MAZUR,[1,*] AND S. K. SUNDARAM[2]

[1]Harvard John A. Paulson School of Engineering and Applied Sciences, Harvard University, 9 Oxford Street, Cambridge, Massachusetts 02138, USA
[2]Ultrafast Materials Science & Engineering Laboratory (U-Lab), Kazuo Inamori School of Engineering, The New York State College of Ceramics, Alfred University, 2 Pine Street, Alfred, New York 14802, USA
*Corresponding author: mazur@seas.harvard.edu

Received October 10, 2014; revised July 15, 2015; accepted July 17, 2015; published October 26, 2015 (Doc. ID 224685)

We present an overview of the different processes that can result from focusing an ultrafast laser light in the femtosecond–nanosecond time regime on a host of materials, e.g., metals, semiconductors, and insulators. We summarize the physical processes and surface and bulk applications and highlight how femtosecond lasers can be used to process various materials. Throughout this paper, we will show the advantages and disadvantages of using ultrafast lasers compared with lasers that operate in other regimes and demonstrate their potential for the ultrafast processing of materials and structures. © 2015 Optical Society of America

OCIS codes: (320.2250) Femtosecond phenomena; (350.3390) Laser materials processing
http://dx.doi.org/10.1364/AOP.7.000684

Ultrafast laser processing of materials: a review

KATHERINE C. PHILLIPS, HEMI H. GANDHI, ERIC MAZUR, AND S. K. SUNDARAM

1. INTRODUCTION

Ultrafast lasers have been developed over half a century and are becoming more user-friendly and less costly every year. As laser researchers continue to advance beyond the attosecond ($1\,\text{as} = 10^{-18}$ s) regime [1], the lasers in the femtosecond ($1\,\text{fs} = 10^{-15}$ s), picosecond ($1\,\text{ps} = 10^{-12}$ s), and nanosecond ($1\,\text{ns} = 10^{-9}$ s) time regimes have been used to interact with and characterize hosts of different materials. Compared with longer pulse widths, ultrafast pulses are unique in that they are characterized by incredibly high peak intensities and interact with materials on a timescale faster than lattice disorder and heat diffusion do. These two features allow ultrafast lasers to very precisely control and manipulate the states of materials.

Over the past few decades, several factors have increased interest in applications of ultrafast processing of semiconductors [2]. Across industries, feature sizes are becoming smaller, and components are becoming more densely packed, which requires ultrafast lasers to precisely machine and manipulate. Along with smaller devices, several applications employing ultrafast lasers have been established that have given more attention to ultrafast laser processing, including automobile machining and photomask repair [3]. Last, with the development of turnkey ultrafast systems that are easier to use, more research with ultrafast laser–matter interactions is occurring across disciplines, while industrial users are exploring more avenues for ultrafast application processing.

In this review, we will first briefly introduce the history of ultrafast laser processing of materials, particularly semiconductors. Next, we will present an overview of the fundamental physical processes that occur in ultrafast light–matter interactions. Then, we will discuss various surface modification, bulk modification, and deposition applications of ultrafast laser processing.

1.1. Femtosecond Laser History

Early laser processing of materials [4] used excimer lasers, which emit pulses of light in the ultraviolet (UV) spectral range. They were used for lithography in the early 1980s. The creation of mode-locking, i.e., fixing the phase between the longitudinal modes in a laser cavity, transformed the laser industry in 1964 and made the generation of picosecond pulses possible for the first time [5,6]. Shorter picosecond pulses brought higher peak intensities, and these new picosecond pulses brought intensities on the order of 10^9 W/cm^2. To amplify picosecond pulses and extract these higher energies, the nonlinear effects that occur at such high powers first need to be taken into account [7]. As the intensity is spatially dependent, the nonlinear phase also changes over the length of the pulse. For a Gaussian-shaped pulse, the nonlinear phase will be the largest in the center of the pulse where the intensity is the highest. This phase results in a spatially dependent nonlinear refractive index. With a larger index in the center, the pulse acts like a lens and self-focuses. The process of self-focusing damages the lasing crystal at high enough intensities.

Chirped pulse amplification was developed to amplify the pulses while keeping the nonlinear effects from destroying the crystal [8]. This amplification process consists of three steps: pulse spreading, amplification, and pulse compression (Fig. 1) [9]. By spreading the pulse orders of magnitude (usually about 10^4–10^8 times), the pulse can be amplified in the crystal without approaching the damage threshold or having intensities, where nonlinear effects come into play [10]. With a spread pulse, the fluence remains the same, but the power measured at any one frequency is much lower. After amplification, the pulse is then compressed.

The process of spreading and compressing the pulse can be achieved with many configurations, such as gratings, prisms, or lenses. The first spreader was designed in 1985 using an optical fiber for spreading with parallel gratings for compression and was improved upon by perfectly matching the spreader and compressor in 1987 [10,11]. With shorter incoming pulses come pulses with very large bandwidths. By dispersing the pulse with the spreader, the pulse becomes chirped, meaning that the many frequencies in the bandwidth are separated in time. The chirp is developed by a combination of self-phase modulation and group velocity dispersion. Through the development of chirped pulse amplification, ultrafast lasers have moved to higher repetition rates, higher powers, and shorter pulse lengths.

A fiber chirped pulse amplified (FCPA) laser system can operate at high levels of the nonlinear phase shift and still provide high-peak-power, high-quality pulses [12,13]. The fiber lasers are based on passively mode-locked fiber oscillators that are then amplified in several stages to reach the desired output pulse energies. Commercially available rare-earth (e.g., Er and Yb) fiber lasers emit in the 1.55 and 1.05 μm wavelength ranges, respectively. With fiber-laser-pumped parametric amplifiers with a peak power over ~10 GW being developed, these systems will become increasingly used for micromachining, imaging, and frequency comb applications [14].

Figure 1

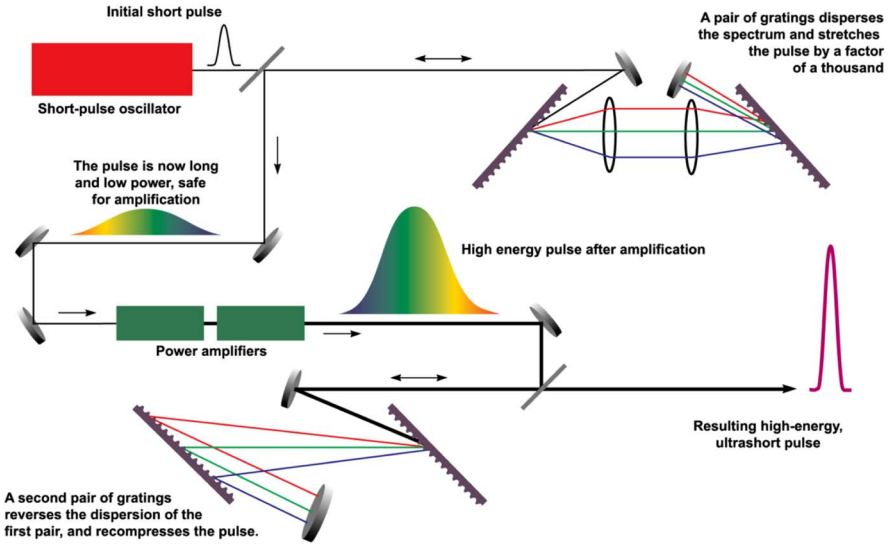

Schematic of beam stretching, amplifying, and compressing system used in chirped pulse amplification. This process is one of the breakthroughs that enabled the creation of ultrafast lasers. Adapted from [9] with permission from Lawrence Livermore National Laboratory.

2. PHYSICAL PROCESSES IN LASER IRRADIATION

The fs-pulse lengths dictate the kinetics of melting and resolidification of materials. A more detailed review of the fundamental dynamics for semiconductors is available in Ref. [15]. Upon fs-pulse irradiation, the semiconductor experiences several regimes of excitation and relaxation, before returning to its original equilibrium state. The four regimes are 1) carrier excitation, 2) thermalization, 3) carrier removal, and 4) thermal and structural effects as detailed in Fig. 2 [15]. Due to the nature of ultrafast pulses, we also describe the resulting differences when compared to shorter, ns-laser pulses. The fs-laser pulses generate large peak electric fields, which are orders of magnitude larger than the 10^9 V/m Coulomb fields that bind electrons to atoms [16]. Large peak pulse energies cause nonlinear absorption in short absorption depths from the irradiated surface, which limits the focal volume where laser energy is deposited.

The dynamics of sub-ps-pulse interactions with semiconductors are unique in two ways. First, the pulse delivers energy to the material on a timescale shorter than the electron–phonon coupling relaxation time. The incident pulse only delivers energy to the electrons, leaving the ions completely "cold." Thermal energy transfer to the lattice only takes place once the pulse is turned off. Thus, decoupled optical absorption and lattice thermalization processes uniquely characterize sub-ps-pulse–semiconductor interactions. Second, extremely short pulse widths in time translate to very high peak intensities that can drive nonlinear and multiphoton absorption processes.

During multiphoton absorption, bonds between electrons in the irradiated sample are directly broken. This is a nonthermal process with no or minimal heating of the sample. Such cold ablation can be attained with laser (not ultrafast) pulses, but only by employing a deep UV wavelength [17]. Multiphoton absorption facilitates absorption in materials with low linear, optical absorption (i.e., wide bandgap semiconductors) that are difficult to machine with traditional ns lasers [17]. The sample surface absorbs the front part of the fs-laser pulse. The extreme electronic excitation creates a dense

Figure 2

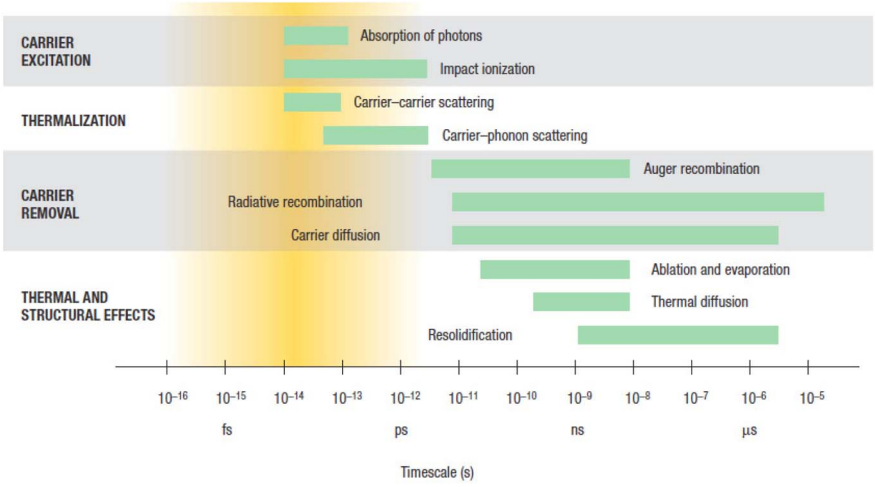

Timescales of four electron and lattice excitation regimes following ultrafast laser semiconductor interaction [15]. For each process, the green bars represent a range of time durations for carrier densities varying from 10^{17} to 10^{22} cm^{-3}.

electron-hole plasma, which is responsible for the absorption and partial reflection of the remaining pulse [18–20]. The plasma then delivers energy to the lattice. Surface interatomic bonds are weakened due to the high degree of electronic excitation, and the lattice is disordered through cold atomic motion. The sample enters an extreme nonequilibrium state with a several thousand kelvin electron gas inside a room-temperature lattice [16]. What happens post-absorption can vary dramatically, depending on the target material's relationship with pulse wavelength and energy [16]. Three resulting regimes are possible: 1) nonthermal melting through an ultrafast phase transition, 2) thermal phase melting, and 3) ablation:

1) Nonthermal melting: A pulse energy large enough to rip 10%–15% bonded valence electrons and achieve a critical density of conduction band electrons (10^{22} cm^{-3}) will induce a nonthermal ultrafast phase transition [16].
2) Thermal phase melting: If the pulse energy does not cause such sudden disordering of the lattice, the plasma energy will spread via electron–phonon coupling to the lattice over several picoseconds [15]. This heat from the excited surface diffuses inward, raising the local lattice temperature. If the solid temperature exceeds its melting temperature, a thin layer near the surface transitions to a liquid state, called the melt. The melt depth increases with laser energy.
3) Ablation: Large pulse energies cause boiling at the melt surface. The resulting superheating of the liquid phase and high nucleation rates of the gas phase eject material from the surface in a process known as ablation.

Specific experimental parameters, primarily laser wavelength and pulse length, determine the fluence thresholds for melting and ablation for a given material system.

2.1. Melting and Resolidification

After irradiation, a thin molten layer forms atop the substrate at room temperature. The corresponding thermal gradient drives the heat away from the molten layer and initiates a fast moving resolidification front, which advances from the substrate toward the top surface. The time interval between irradiation and resolidification is several nanoseconds [15].

The resolidification-front speed determines the chemistry, crystallinity, and morphology of the resolidified layer. For silicon, a front speed faster than the liquid to crystal relaxation rate (∼15 m/s) will deprive atoms enough time to find their equilibrium positions, yielding an amorphous material. A slower resolidification front will cause a longer lasting molten phase and epitaxial regrowth with a crystalline resolidified layer [21].

Higher laser fluences lead to longer melt durations and slower resolidification fronts. Laser pulse exposure just above the melting threshold causes the material to resolidify as an amorphous solid. At higher fluence thresholds, melting is typically followed by growth of crystalline structures.

2.2. Ablation

The process of ablation occurs when the fluence of the laser light exceeds that of the ablation threshold. For fs-laser–matter interaction, the laser pulse duration is much shorter than the electron-cooling rate, which has been shown to be on the order of 1 ps [22]. With high laser fluences, energy from the surface of the material causes some of the surface melt to evaporate in the form of an ablation plume. Research into the ablation process has shed light on the mechanism. By modeling the fluidic

movements of the melt, it has been shown that the ablation occurs from fragmentation of a supercritical volume expansion in a short time frame [23].

When the laser fluence exceeds that of the ablation threshold, we can achieve laser-induced periodic surface structures (LIPSS) [24]. For fs-laser texturing, the LIPSS formed consist of semi-periodic nanometer- and micrometer-scale structures [25–27]. The LIPSS are independent of the crystal orientation and exhibit a wide range of feature sizes and shapes. The formation of LIPSS in the shape of ripples occurs when surface waves in the melt develop as the incoming light interferes with the scattered light off of the material. As more pulses impinge on the ripples, self-focusing occurs in the valleys and can result in larger structures that go deeper into the material. For this process, LIPSS are created that are dependent on the wavelength and polarization of the incoming fs-laser pulse and the index of refraction of the host material that is being textured [28].

Derrien *et al.* have investigated the mechanisms of LIPSS formation under fs-laser irradiation of silicon in air and silicon in water [29]. In air, the authors have observed low-spatial-frequency LIPSS (LSFL) with periods somewhat smaller than the laser wavelength ($\Lambda_{\mathrm{LSFL}} \sim 0.7 \times \lambda_0$) and an orientation perpendicular to the laser polarization. Surface plasmon polaritons (SPPs) have been proposed as a mechanism to explain the formation of the near-wavelength ripples that occur when a small number of intense pulses irradiate materials at intense and reduced numbers of pulses in various materials. In the case of metal, the ripple formation mechanism has been linked with the excitation of surface plasmons. But in the case of semiconductors or dielectrics, transitory metallic states follow plasma dynamics of the free-carrier gas, and nanometric defects (e.g., bubbles and nanoparticles) correspond to localized surface plasmon (LSP) excitation. Under the SPP excitation, electron-hole pairs are generated along with thermal effects. The results of Derrien *et al.* [30] show that the SPPs can be excited by using a fs laser with 800 nm wavelength, 100 fs pulse duration, and laser fluences larger than 0.7 $\mathrm{J/cm^2}$. A comparison of the calculated SPP periodicities and experimentally measured ripple periodicities confirms that the formation of periodic structures with a reduced number of laser pulses is due to the excitation of SPPs at the Si surface.

In the case of laser processing in water [29], a reduced ablation threshold and LIPSS with approximately five times smaller periods $\Lambda_{\mathrm{LIPSS}} \sim 0.15 \times \lambda_0$ have been observed in the same direction as in air. The authors have used the experiments using 100 fs-laser (790 nm) pulses per spot and showed that the LIPSS in water are formed at smaller fluence values, as the ablation threshold in water is reduced by several tens of percent due to absorbed fluence in the sample. Therefore, the LIPSS periods are significantly reduced, typically by a factor of five reaching periods between 80 and 130 nm. This behavior originates from the SPP excitation in the presence of a 10–20 nm thick silicon oxide layer and the optical excitation of water.

When it comes to ablation, we see that femtosecond lasers can damage even the hardest known materials [31]. Because ablation is such a destructive process for the irradiated material, we can use ablation to our own advantage across industries. Ablation is one of the easiest ways to cut and scribe hard materials. Fs-laser ablation also leads to self-organized nanostructures in fluoride crystals [32]; e.g., spherical nanoparticles of ~100 nm diameter can be formed using circular polarization. The ablation results in a transient perturbation of the material to a state far from equilibrium. Upon ultrafast relaxation in a few picoseconds, self-organized surface patterns of feature size $\leq$100 nm can develop, depending on the deposited energy dose and the polarization of the incident light [33]. Recent results on fs LIPSS on silicon demonstrate the LIPSS formation via irradiation with a fs white light continuum

and the dose dependence of pattern evolution at about threshold fluence of the material. Reif *et al.* [34] have proposed a dynamic model to explain the self-organization process. One can describe the irradiation-dose-dependent evolution of corrugation height h:

$$\frac{\partial}{\partial t}h(x,y,t) = -\nu(\varphi,\theta)\sqrt{1+(\nabla h)^2},$$

where v is the ablation velocity that depends on the laser fluence. Due to several competing processes, the system will behave nonlinearly with increasing excitation. One can use the Kuramoto–Sivashinsky type of equation to describe the corrugation evolution:

$$\frac{\partial h}{\partial t} = \nu_o + \nu\Delta h + \lambda(\nabla h)^2 - K\Delta^2 h + \eta,$$

where v_o is the ablation velocity. The second term denotes the linear dependence of the ablation rate on the surface corrugation. The third term denotes the nonlinear contributions to erosion at increasing corrugation. The fourth term stands for the loss of corrugation depth by diffusion. The last term denotes the initial surface roughness. The experimental results compare well with the prediction of the model.

Since fs-laser ablation acts on a faster timescale than the time it takes for the thermal energy to diffuse into other areas of a material, we can use ablation to remove material in very precise ways in three dimensions. These dynamics are illustrated in Fig. 3 [35]. We will discuss the positive attributes of fs-laser ablation in many applications in the section below.

3. COMPARISON WITH THE NANOSECOND REGIME

Nanosecond pulses excite electrons in a distinctly different process as compared to the fs excitation. When a ns pulse delivers energy to a material, excited electrons transfer energy to the lattice during the time of the electron excitation. Electrons and the lattice thus remain in equilibrium throughout the excitation process. The ns laser heats the solid to its melting temperature during the length of the laser pulse [15]. The ns-absorption processes are linear with a much larger absorption length than fs absorption. Linear absorption can lead to deeper melt depths. Compared to the fs-laser case, the ns-induced temperature gradient between the molten layer and the solid substrate is smaller and distributed over a longer distance. Consequently, the melt duration is longer, and the resolidification-front speed is slower, which for silicon typically yields a crystalline structure. If the laser wavelength is transparent to the material, absorption is induced by multiphoton absorption for both ultrafast and ns lasers. Then the ns laser will have a longer penetration depth due to a smaller absorption cross section as compared with an ultrafast laser. In contrast, for the opaque materials, the penetration depth is determined by the absorption coefficient due to single-photon absorption for both lasers. In the case of a small absorption coefficient, a shorter penetration depth of the ultrafast laser may be obtained due to a combination of linear and nonlinear absorption.

The longer ns-pulse widths translate to lower peak powers compared to fs lasers. Operating at lower peak powers, ns lasers ablate materials by a thermal process [17]. This thermal ablation (Fig. 3) causes a large heat-affected zone that may induce melt redeposition and shockwaves, leaving behind thermally induced defects such as cracks and chipping [36,37].

Figure 3

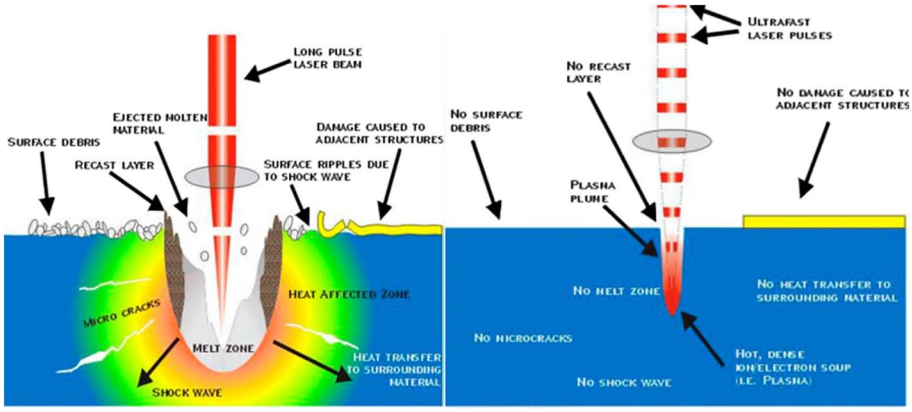

Comparison of the ns-ablation (left) [37] and the fs-ablation (right) [35] processes. In machining or surgery applications, the thermal effects in ns ablation can lead to a larger heat-affected zone, more collateral damage, and less precise machining compared to fs ablation. Each figure used with permission from Clark-MXR, Inc.

4. APPLICATIONS

There are a wide variety of applications when it comes to fs-laser processing of materials. In this paper, we will explore three types of applications: 1) surface modification, 2) bulk modification, and 3) deposition techniques. We will focus on electrical and energy applications and not touch on the bioapplications due to the breadth of the disciplines covered [38]. Fs lasers are also used as material characterization tools, and many other studies detail their uses in fs pump-probe spectroscopy [39,40], laser-induced breakdown spectroscopy (LIBS) [41], and surface-enhanced Raman spectroscopy (SERS) [42].

4.1. Surface Modification

One of the main applications of fs lasers is surface modification. In this section, we first discuss texturing the surface for applications including light trapping and hydrophobicity. Next we discuss machining applications in which the laser is employed to scribe and drill through semiconductors. Last, we will discuss the use of fs lasers to hyperdope, that is, dope beyond a material's equilibrium solubility limit.

4.1a. Surface Texturing

The surface structures made from fs-laser texturing of semiconductors can be applied to a variety of applications, including light trapping and hydrophobicity. Femtosecond lasers have been used to produce a wide variety of surface structures including conical peaks [16,43], periodic gratings [44,45], and ripples [46,47]. Light trapping is the most important when absorption is the main application, such as in a solar cell or photodetector. For this reason, light trapping has been studied mostly in silicon, as it constitutes the vast majority of solar cells and photodetectors produced. In order to maximize the light absorption for a device, light trapping takes advantage of the photons that are energetic enough (above bandgap) for the host material to absorb but have scattered from the surface and hence are unusable. The common solution to light trapping is to use an antireflective coating, usually silicon nitride, but that still leaves about 10% unabsorbed light [48]. It is for this reason that using fs-laser texturing of silicon has become an important field of study. The texturization produces a polycrystalline layer approximately 100 nm thick near the surface, which exhibits a low minority carrier lifetime. By removing this layer, the efficiency of a photovoltaic device can be improved [49]. Ns lasers have also been used to create structures in Si for light

trapping. Due to the slower resolidification-front velocity, no polycrystalline layer is observed on the surface [50].

By comparing many different types of texturing on silicon, research has shown that fs-laser-textured silicon has less overall scattering than chemically textured silicon with silicon nitride [43,51,52]. However, the internal quantum efficiency (IQE) of the chemical texturing plus silicon nitride is still higher than the laser-textured sample, which shows that the texturing aids light trapping but also hurts the overall efficiency. A device optimization study has shown that laser-texturing silicon in SF_6 allows for the creation of thin-film solar cells because more photons can be absorbed with a thinner absorption layer (~20 μm) [52]. The study also found that the absorption from laser texturing approaches the theoretical limit for solar cell absorption, or the Yablonovitch limit, and has worked on making a solar cell with laser texturing as a basis for the solar cell's light trapping [52,53].

In addition to light trapping, the same laser-irradiated silicon surfaces have been shown to be hydrophobic, with applications in biology and materials science. Femtosecond-laser texturing of silicon in SF_6 yields micrometer-sized spikes, which many groups have used to increase the contact angle, which is the angle formed by a liquid placed on the surface of a material. Studies first showed that by varying the laser fluence, it was possible to control the resulting contact angle and hence the hydrophobic properties of the underlying silicon [54]. Through subsequently layering molecules, such as fluoroalkylsilane, on the laser-textured silicon surface, it was later shown that the surface molecules increased the contact angle further, making the surface even more hydrophobic [55]. With both light trapping and hydrophobic properties, laser-textured silicon yields a surface that can be used in a variety of applications—many of which remain unexplored.

4.1b. Machining

Ultrafast lasers are among the highest performing tools to perform surface modification machining. Micromachining refers to the creation of micrometer-scale features such as holes, lines, and grooves within and on the surfaces of materials. Ideally, these features are produced with minimal peripheral damage. Historically, laser micromachining in semiconductors has been carried out with diode-pumped solid-state or excimer lasers with ns-pulse durations [2,17]. However, the effects of thermal diffusion that stems from ns-laser machining place a lower limit on the length scales that can be machined. Furthermore, thermal diffusion can lead to poor machining quality and a large heat-affected zone, which can induce detrimental stresses, cracks, molten layer recast, and slag [2].

Femtosecond lasers offer a new paradigm in machining quality with high spatial resolution and minimal thermal damage. With their ultrashort pulse lengths, fs lasers can deposit energy to a material in a controllable manner on a timescale faster than ps-electron–phonon coupling processes [56]. Heat diffusion into the machined-area periphery is minimal and leaves behind a small amount of molten material [36]. This small heat-affected zone contains a low level of thermal defects, which are common in ns-laser processing, such as cracking and chipping.

Compared to traditional Q-switched solid-state lasers and nanosecond lasers, fs lasers have an overall higher cost of ownership. As such, industrial adoption of fs lasers has been limited to high value-added applications where high precision is required [2]. Picosecond lasers land in the middle, delivering a machining quality that is less precise than fs lasers but suitable nonetheless for many applications [2]. Their lower cost of ownership has made ps lasers a preferred candidate for most commercial applications. In this section, we will discuss three main aspects of machining that are used in industrial applications: scribing, drilling, and dicing.

Scribing. Laser scribing is the process in which a focused laser is scanned across a material surface to form a continuous line or groove, without completely vaporizing through the material. Laser scribing is used to shape a variety of brittle semiconductors across industries. Here we discuss two applications in the photovoltaic industry: scribing of thin-film photovoltaic modules to achieve series interconnections and edge isolation of crystalline silicon modules to remove shunt paths.

Scribing thin-film solar photovoltaic modules is one particular application that can benefit from the small heat-affected zones associated with fs-laser ablation. A thin-film solar module consists of hundreds of series-connected cells, or mini-modules, atop a glass substrate, as shown in Fig. 4 [57,58]. Mini-modules limit module ohmic losses and are interconnected by multiple steps of depositing and scribing an individual thin material layer [58]. Directly after each material layer is deposited, it is scribed before the next layer is deposited. The complete scribing process is shown in Fig. 5 [59]. This scribing process series connects the mini-modules as desired, but it also forms detrimental electrically inactive dead zones between adjacent mini-modules. Reducing the dead zone size, which is fundamentally limited by the area of each scribe, is critical to increasing the overall module efficiency [58].

Due to their precision, repeatability, and small heat-affected zones, pulsed lasers are well suited to achieve effective scribing and minimum dead zone size. Today most thin-film photovoltaics manufacturers use ns lasers for their scribing processes [58]. In the last decade, many groups have demonstrated that ultrafast lasers deliver better scribing performance than ns lasers for thin-film material layers, including copper indium gallium selenide (CIGS) [60–62], cadmium telluride (CdTe) [57], and indium-tin oxide (ITO) [63]. Ultrafast scribing inflicts smaller thermal effects, which minimizes dead zone size, laser-induced defects, and unwanted ablation-induced redeposition on the scribed channel walls that leads to electrical shunts. While ultrafast scribing has shown superior performance to ns scribing, industry adoption has been limited by the ultrafast laser's higher cost, lower output frequency (reducing throughput), and Gaussian profile (which can lead to nonuniform ablation relative to a top hat profile) [58,64].

Another photovoltaic application of scribing is edge isolation. Most crystalline silicon photovoltaic manufacturers form cell p-n junctions by coating a p-doped silicon wafer with an outer n-doped layer via phosphorous diffusion. The edge surface n-doped layer may form an unwanted electrical connection between the front and back contacts

Figure 4

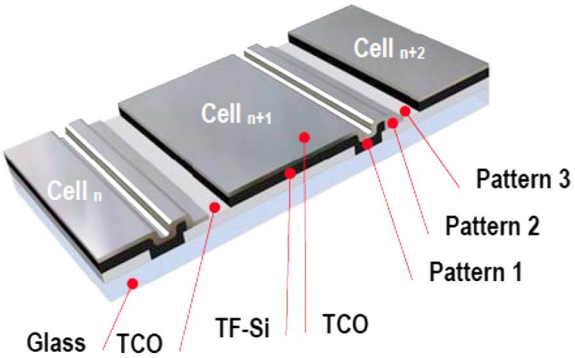

A thin-film module is composed of many series-connected mini cells (i.e., mini modules) in order to limit overall module ohmic losses (which are proportional to the square of the current flowing through one module segment) and provide large overall module voltage output. Reproduced, with permission, from [58].

of the device. This shunt short-circuit path allows the flow of an internal current, robbing photo-generated current from an external load. Edge isolation, shown in Fig. 6, is the process of forming a continuous groove through the n-edge layer that electrically isolates the shunt path [65].

Figure 5

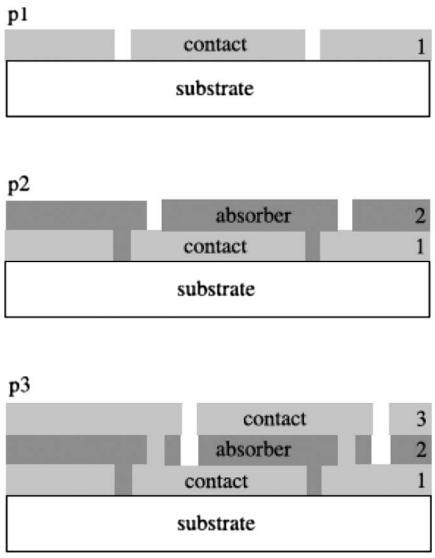

Typical three pattern scribing step sequence employed in thin-film module production. After each layer is deposited on a substrate, it is subsequently scribed; after this, the next layer is deposited. Completion of the third pattern, P3, step results in the formation and series connection (shown in light gray) of many mini modules on a single module. Reprinted with permission from R. Bartlome *et al.*, Appl. Phys. B 100, 427–436 (2010) [59]. Copyright 2010, AIP Publishing LLC.

Figure 6

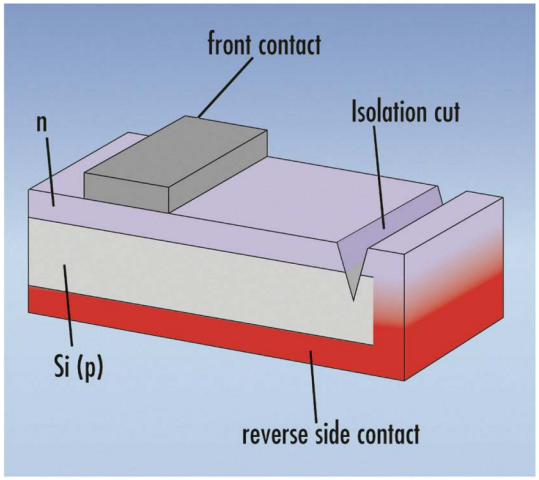

In photovoltaic module processing, an edge isolation cut eliminates the potential shunt path between the p-type wafer and n-type coating that forms an emitter layer. A high-precision cut via an ultrafast laser preserves more electrically active module area, facilitates higher module-processing yields, and promotes a longer module lifetime. Reproduced, with permission, from ROFIN [65].

Various methods, including lasers, plasma etching, chemical etching, are used to achieve edge isolation [66]. Photovoltaic manufacturers employing laser grooving typically use green or UV ns lasers, but scribing with ultrafast lasers offers several advantages [58,66]. The narrower and closer to the edge a groove is, the more cell-active area will be preserved, leading to higher overall device efficiency [17]. Furthermore, precisely forming the groove without unwanted effects, such as edge surface roughness or microcracking, gives rise to higher processing yields and long-lasting module lamination and reliability. Several studies of edge isolation using high-power ps lasers have shown cleaner isolation grooves compared to traditional ns processing [67–71]. Simulations also suggest that such ps processing can be scaled up to industry levels at throughputs faster than current industry standards [67].

Drilling. Another application of fs-laser machining is drilling or milling of materials for industrial applications. After the formation of LIPSS within the laser focal volume, as shown in Fig. 7, we see that the introduction of more pulses, on the order of thousands, leads to drilling a hole with relatively vertical sidewalls [22]. Although most work in this field has been done on metals, the method can easily be extended to semiconductors [72]. Due to fs-laser ablation not involving thermal effects, we can achieve much better micromachining characteristics than with other methods. In comparison to nanosecond lasers, fs-laser drilling yields much more precise holes with less residual damage or redeposited material [73].

This circular ablation can be performed on a wide variety of materials, including silicon and titanium nitride (TiN). In silicon, we see that it is the lack of a liquid phase created with fs lasers that leads to much better hole creation. For ns lasers, a liquid phase is created and leads to unstable drilling and ultimately produces a poorer quality

Figure 7

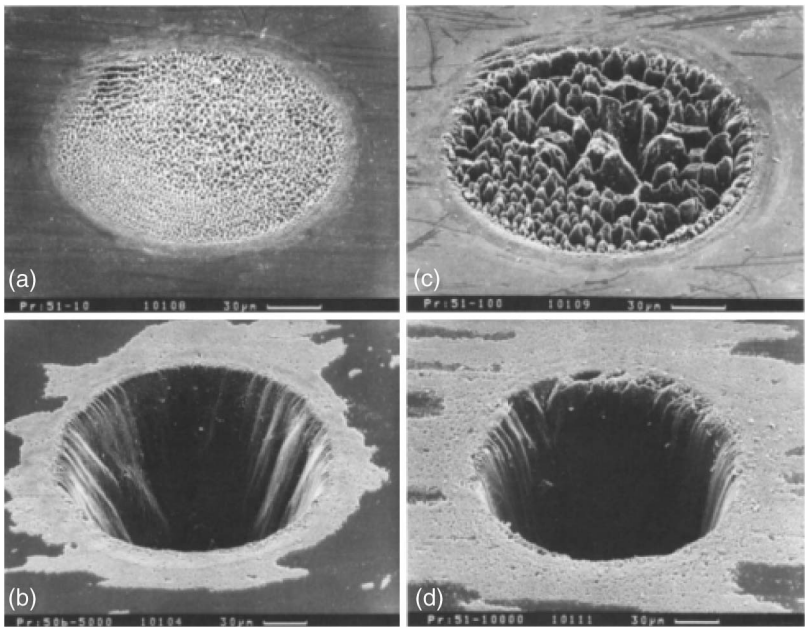

Hole drilling from Ref. [22], showing drilling hole formation via laser ablation of a silicon target with (a) 10, (b) 100, (c) 5000, and (d) 10,000 pulses. Reprinted with permission from N. Chichkov *et al.*, Appl. Phys. A **63**, 109–115 (1996) [22]. Copyright 1996, AIP Publishing LLC.

material [22]. In TiN evaporated and deposited on silicon, TiN can be drilled efficiently with the fs laser. With additional pulses, the underlying silicon can also be structured [71]. It is interesting to note that the drilling can work with a power just above the ablation threshold and that the depth of the hole is linearly dependent on the number of pulses applied [71]. This linear dependence shows that it is the overall number of pulses applied that determines the overall hole depth, and that it does not take large peak powers for drilling in semiconductors to occur. Because the underlying silicon was structured as the number of pulses (and hence the depth of the hole) increased, this method shows that multiple materials in a stack can be drilled with a fs laser.

Dicing. Ultrafast lasers are not only used to machine grooves or holes in semiconductors, but can also cut, or dice, straight through these materials. In the microelectronics industry, dicing is used to separate the many individual integrated circuit chips that are written on a lithographically processed wafer. An image of a wafer with many dies in depicted in Fig. 8 [36]. Historically, the microelectronics industry has used thick wafers (i.e., greater than 150 μm) that could be effectively diced with diamond-coated wire blades that cut via mechanical abrasion. Now the industry demands 50 μm or thinner wafers that could crack, chip, or delaminate in response to mechanical stress from wire dicing. Noncontact laser dicing, however, can effectively dice these thin wafers with higher precision and throughput. Laser dicing offers additional benefits such as reduced dice tool ware, reduced dice contamination, and the ability to curvilinearly form rounded corners on individual dies, which increase die mechanical strength [74].

Studies have found that laser dicing cut quality is dependent on pulse width [74]. Poor-cut quality is largely due to thermal melting and molten layer redeposition for pulse widths larger than 1 ns. Recognizing the minimal thermal effects of ultrafast processing, many groups have investigated high-quality dicing with fs lasers [75–77]. Furthermore, small cut lines from ultrafast dicing are advantageous in that they allow for more circuit chips to be placed on a lithographically processed wafer (produced at a fixed cost), reducing the average cost per chip. Different fabrication procedures such as the use of line foci or employing double pulses have been explored to find optimal conditions that minimize cut widths and maximize cutting speed [76,78,79]. Currently, the major barrier to wider industrial adoption of fs dicing is concern about low fs-laser repetition rates and dicing throughput [74].

Figure 8

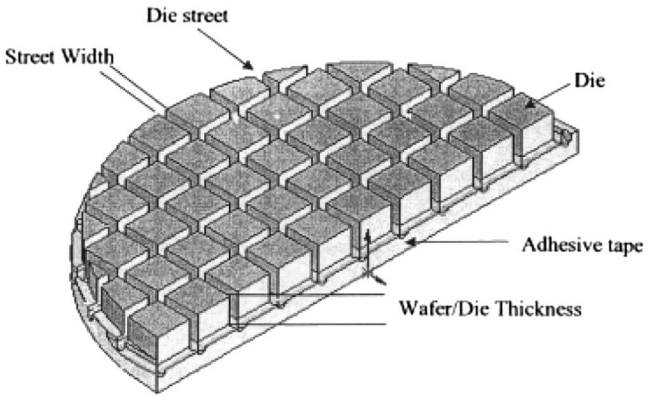

Schematic of a lithographically processed wafer with individual dies electrically isolated from one another by street widths. Each die contains an integrated circuit or device. The overall wafer must be diced to physically separate the dies. Reproduced, with permission, from [36].

4.1c. Hyperdoping

One unique application of fs-laser processing of semiconductors is the ability to hyperdope target materials. Hyperdoping refers to doping semiconductors at concentrations beyond their equilibrium solubility limit without forming compounds or secondary phases [80]. Doping can be achieved through the introduction of dopants, either in the gaseous environment or as an evaporated thin film, while target semiconductors are laser-processed as described above. The fundamental mechanism behind hyperdoping is that molten liquid phases can host more dopants than equilibrium solid phases. Hyperdoping has also been achieved by ion implanting samples and subsequently using a nanosecond laser to remelt the sample and recrystallize the lattice [80,81]. The hyperdoping process was originally developed by irradiating silicon with a train of amplified fs-laser pulses in the presence of a wide variety of dopant precursors [82,83,84]. It has been shown that silicon can be hyperdoped to more than 1 at. % sulfur in a 300 nm thin layer [81]. In addition, the process produces semi-periodic surface textures that have excellent antireflection and light-trapping properties as shown in Fig. 9(a) [85]. At a high chalcogen (S, Se, Te) doping concentration, fs-laser-doped silicon exhibits near-unity light absorptance from the ultraviolet to the near infrared, which is far beyond silicon's bandgap of 1.1 μm [Fig. 9(b)] [85].

Using fs-laser fabrication, research has shown the ability to incorporate dopants at concentrations thousands of times above the solid solubility limit [84]. Fs-laser hyperdoping achieves this through a process called solute trapping [16,86]. Laser pulses that have energies greater than the melting threshold transform the surface into a molten layer, which enables dopants to diffuse in. As the deposited energy diffuses into the substrate, the molten layer resolidifies with a speed greater than the dopants can diffuse out (>1 m/s), which traps the dopants in, thus resulting in supersaturated concentrations [87]. Such high dopant concentrations should yield an intermediate band in the semiconductor bandgap [88]. In addition to doping, the creation of conical surface structures as discussed previously aids in light trapping for the hyperdoped materials, and work in silicon has recently identified laser parameters for independently tuning the hyperdoping and texturing processes [16].

The work with ion implantation and subsequent ns-laser melting has been extended to a variety of transition metals, where an infrared silicon photodetector hyperdoped with gold has been successfully achieved [89]. This ns-hyperdoping method produces hyperdoped layers with better crystallinity versus fs-produced hyperdoped layers, albeit at lower dopant concentrations with less sub-bandgap absorption. The method

Figure 9

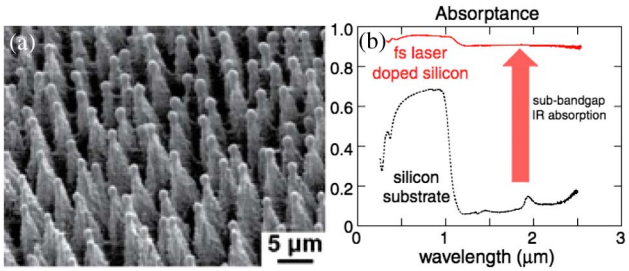

(a) Spiky, high-aspect-ratio, laser-induced periodic structures in silicon upon exposure to SF6 and fs-laser irradiation [85]. (b) Absorption enhancement due to black silicon light-trapping conical tips and hyperdoping. Hyperdoping leads to strong sub-bandgap absorption, and texturing leads to increased absorption across the spectrum [85].

has been used to produce silicon-based photodiodes with a large response to photon energies down to 0.7 eV, which is below that of commercially available silicon-based photodiodes, which are limited by silicon's 1.1 eV bandgap [90]. Figure 10 shows the microstructure of the Si surface produced by a ns laser, which shows spikes with somewhat rounded tips. The surface layer contains about 1 at. % of sulfur, which acts as a dopant in the laser-etched layer. Hall measurements of this layer show a higher electron concentration than the substrate and electron mobility on the order of 100 $cm^2\ V^{-1}\ s^{-1}$. The ns-laser irradiation creates an $n/n+$ heterojunction between the undisturbed crystalline substrate and the disordered surface layer [90]. SiOnyx, Inc., is currently commercializing infrared photodetectors for military and consumer electronic applications utilizing piscosecond texturing of silicon [91].

Fs hyperdoping has also recently been demonstrated in larger bandgap oxide semiconductors titania (TiO_2) and zinc oxide (ZnO). Both demonstrations have shown the incorporation of defect atoms into the oxide lattice and glassy materials [92–94]. In the case of ZnO, antimony (Sb) was even incorporated in a single crystal portion of the laser-modified surface region as shown in Fig. 11 [94]. By utilizing both the hyperdoping and surface texturing process of fs-laser processing, many new fields can be explored across many material platforms.

4.2. Bulk Modification

After discussing many applications in surface modification, we now will move onto techniques using fs lasers to modify the bulk materials. The two applications we will discuss in the next section are 1) annealing to crystallize the lattice and 2) direct patterning. As with the surface modification, many different groups use fs lasers to fundamentally change the bulk properties of a material and ultimately create states or substances that cannot be produced using other known methods.

4.2a. Ultrafast Bulk Annealing

Semiconductor annealing refers to heat-treating a material to alter its crystallinity and resultant physical properties. Annealing traditionally refers to a series of equilibrium kinetics processes that heat a material beyond its melting temperature, maintain the temperature, and subsequently cool the material. Here we focus on highly nonequilibrium ultrafast annealing used to improve crystallinity and material performance.

The microelectronics and photovoltaic industries have historically used furnaces for thermal annealing and rapid thermal annealing to improve the crystallinity of polysilicon grown from deposited amorphous silicon [95]. However, because they operate via

Figure 10

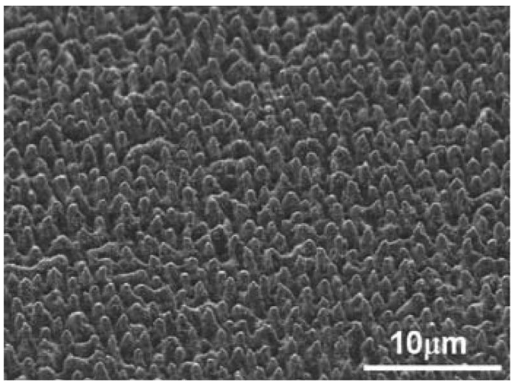

SEM of microstructured Si surface using a ns laser [90].

bulk heating, both methods cannot selectively heat a specific layer within a multilayer stack, constraining the type of material layers and substrates that can be used. To overcome these limitations, the microelectronics industry has begun using microsecond annealing, via flash lamps or continuous wave diode lasers, to achieve selective heating and to activate shallow dopants following host lattice ion implantation damage [96].

Laser annealing on ultrafast timescales allows for even more precision in selectively heating a stack of materials. Aside from being confined to a more precise focal volume, ultrafast crystallization is advantageous in that it can be done while simultaneously ablating a surface. This stems from the nonlinear absorption and nonequilibrium light–matter interaction discussed above.

The low fs-ablation threshold has been exploited to demonstrate simultaneous crystallization and surface texturing of 1.5–2.5 μm thick a-Si films deposited on glass [97]. Further studies have characterized the effect of laser parameters on the resulting spike formation, absorption, and crystallinity on similarly processed amorphous samples irradiated in air and water environments [98]. One study reports that the crystallization forms a blend of hydrogenated nanocrystalline (nc-Si:H) and a-Si:H that improves material stability in the face of light degradation [98]. The high amount of resulting structural defects, however, currently limits this technique from being deployed in photovoltaic applications.

Crystallization with ps lasers has also recently been explored to potentially make an a-Si:H/nc-Si:H micromorph tandem cell [99]. Such a tandem cell is shown in Fig. 12(a) [99]. In this process, a deposited a-Si:H layer is partially converted to a polycrystalline layer via ps-laser annealing as shown in Fig. 12(b) [99]. Such a fabrication procedure would simplify and complement the current multistep chemical vapor deposition (CVD) growth process.

4.2b. Direct Patterning

One of the most transformative fs-laser applications is to utilize the two-photon process to micromachine the bulk of the materials yielding structures in three dimensions

Figure 11

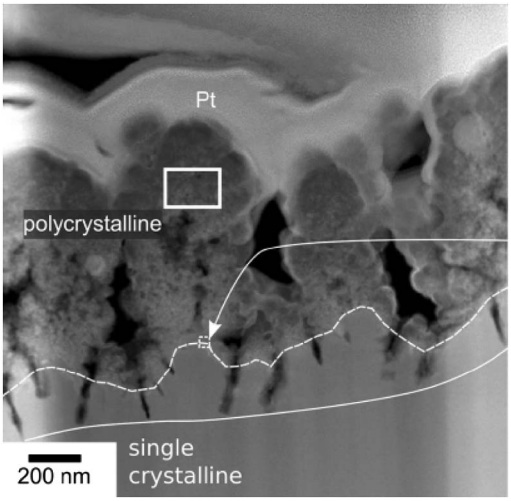

This TEM image reveals how fs hyperdoping has introduced antimony in a crystalline layer of ZnO. Reprinted with permission from A. Schneider *et al.*, J. Appl. Phys. 113, 143512 (2013) [94]. Copyright 2013, AIP Publishing LLC.

(3D) [100]. Fs-laser processing allows for the direct patterning of a variety of materials and the creation of large structures in 3D. Micromachining was first developed in transparent materials, such as SiO_2 [101,102]. Due to using two- or multi-photon processes, most research in micromachining has focused on polymers and soft materials as well as glasses [103,104].

However, it has been shown that it is possible to pattern TiO_2 by irradiating a photosensitive sol-gel TiO_2 with below bandgap light. The incoming light initiates a multiphoton process that is able to break down the resist. The resulting structure can be quite complex, such as the woodpile shown in Fig. 13 [105]. Silicon has also been micromachined with fs lasers, which results in a reduced heat-affected zone when compared to ns lasers, leading to less induced stress [106].

Another use of micromachining in semiconductors makes use of the proliferation of 3D-patterened polymers by coating the resulting polymer 3D structure with semiconductors to form 3D semiconductor patterns. Recently, CVD was used to deposit a thin silicon layer over an underlying 3D polymer pattern to create a 3D silicon woodpile photonic crystal structure [107]. By coating semiconductors onto polymer patterns, we can access a much larger range of materials and structures that are normally too complex to make from mainstream semiconductor processes.

4.3. Deposition Techniques

Last, we will cover various applications in deposition techniques that make use of fs lasers to ablate various materials and then redeposit the ablated material onto additional substrates. By altering the target material and the surrounding environment that the ablation occurs in, many different types of semiconductors can be formed. Here, we will discuss 1) nanoparticle formation from the ablated particles, 2) pulsed laser deposition, which creates films from the ablated particles, and 3) laser-assisted growth, where the ablated particles are used as seed material to deposit other materials. In each of these cases, fs-laser ablation helps to create materials that other deposition

Figure 12

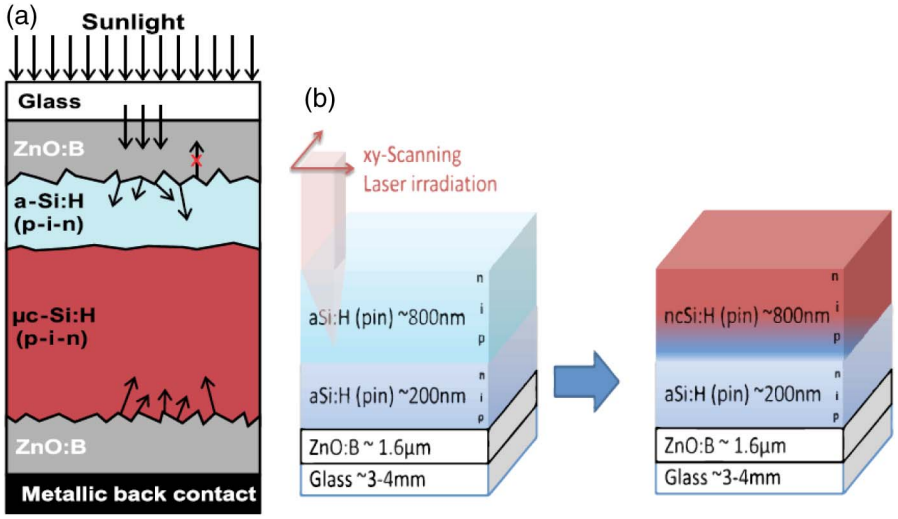

(a) a-Si:H/nc-Si:H micromorph tandem cell, currently grown by CVD. (b) Proposed alternative fabrication method to produce the micromorph tandem cell in fewer process steps by utilizing ps-laser annealing. Reprinted with permission from I. Theodorakos *et al.*, J. Appl. Phys. 115, 043108 (2014) [99]. Copyright 2014, AIP Publishing LLC.

techniques struggle to make with high precision. Ns lasers have also been used for deposition processes. For example, Mirza and coworkers [108] have compared the ns- and fs-pulsed laser-based PLD of silver nanoparticle films of 1–7 nm thickness deposited on fused quartz. The ns-PLD nanoparticles are well separated and somewhat spherical up to ∼3 nm thickness, beyond which the particles coalesce and then result in a percolated structure at ∼7 nm. In the fs-laser case, the nanoparticles are also well separated, but the mean particle size and the surface coverage increase with equivalent thickness. The behavior is attributed to a difference in plasma formation. The ns plume is almost fully ionized plasma, while the fs laser ablates the material with a small fraction of particles in plasma state.

4.3a. Nanoparticle Formation

Fs-laser irradiation of semiconductors beyond the ablation threshold produces ablated particles. We can utilize this material in the form of nanoparticles [109]. In order to gather the nanoparticles, the setup usually involves positioning a target material at a 45° angle in relation to the incoming laser beam with a collection substrate positioned parallel to the target material [110].

For silicon, nanoparticles can be formed in a vacuum [111] or in a gaseous atmosphere containing gases, such as H_2 [112]. It has been shown that the ablation of silicon nanoparticles has a large size distribution that clusters into aggregates and webs that are 5–300 nm in size [112]. By changing the atmospheric gas to H_2S, the size of the ablation plume cone also changes. The phase of the formed nanoparticles can be either crystalline or amorphous, which is determined by the cooling rate of the ablated silicon in the liquid phase. When a gaseous atmosphere is present, the gas forces some nanoparticles to cool through a thermal process and hence not go through a nonthermal phase transformation [112]. For silicon ablated in a vacuum, the nanoparticles cool at a much faster rate and do not have the gas in the atmosphere to compete with, leading to only nanoparticles and clusters and not the formation of webs. Hence, the resulting nanoparticles are dependent on many factors in the ablation and subsequent cooling process.

Recent results show that better nanoparticles can be synthesized in different environments, e.g., ultrafast laser ablation in liquids [113]. By varying the intensity of fs-laser

Figure 13

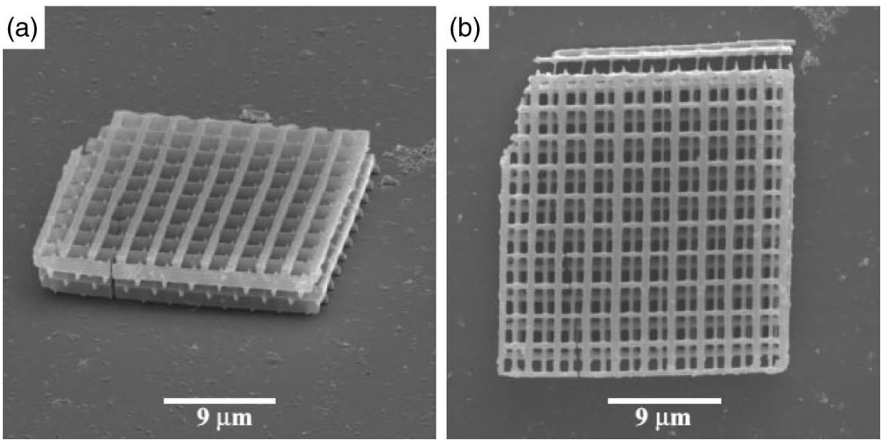

SEM Images of fs-laser 3D structured TiO_2 in a woodpile formation shown from two different angles. S. Passinger *et al.*, Adv. Mater. 19, 1218–1221 (2007) [105]. Copyright Wiley-VCH Verlag GmbH & Co. KGaA. Reproduced with permission.

radiation, the size of nanaoparticles can be controlled. For example, the mean size of gold nanoparticles can be reduced from 120 to 4 nm by the decrease of laser fluence down to the threshold values or changing the radiation focusing on the target surface. In the fs-ablation regime, much less radiation energy is transferred to the cavitation bubble (15% compared to 80% in the ns-laser pulse regime). This avoids the cavitation phenomena, leading to uniform fine nanoparticles. Use of biopolymers and oligosaccharides liquids leads to drastic reduction of the nanoparticle size down to 3 nm with the size dispersion not exceeding 1.5 nm FWHM as they react with laser-synthesized gold nanoparticles. This is due to the hydrogen bonding of the—OH groups of these compounds and the—O- at the gold surface. The OH groups of different biocompatible compounds can efficiently react with the oxidized gold surface, leading to the reduction of the nanoparticle size. In addition, the ultrapure laser-ablated nanoparticles can be functionalized by a proper chemical modification of chemicals, solving the toxicity problems associated with these particles.

4.3b. Pulsed Laser Deposition

By extending the process of nanoparticle formation, we can make thin films of materials through pulsed laser deposition (PLD). Through a similar setup to that for nanoparticle formation, complex materials can be deposited onto a variety of substrates [114]. The main advantage of PLD over other deposition techniques is its ability to repeatedly grow thin films with precise and complex stoichiometries.

The most common use of PLD is for deposition of thin films. In order to deposit an oxide, the fs laser is used to excite plasma on the target material, and then the nanoparticles fly off onto a flat substrate. To deposit tin oxide (SnO_2), the amount of background oxygen gas was instrumental in producing high-quality epitaxially grown films, even though they started with a target that already contained the correct amount of oxygen, SnO_2 [115]. Another example of thin-film PLD is the creation of cadmium sulfide (CdS), where it was shown that the substrate used, between silicon and quartz, determines the quality and grain size of the material deposited [116].

A variety of photovoltaic absorber materials [e.g., CdTe, zinc sulfide (ZnS)] and transparent conductive electrode materials [zinc oxide (ZnO), ITO] have been produced

Figure 14

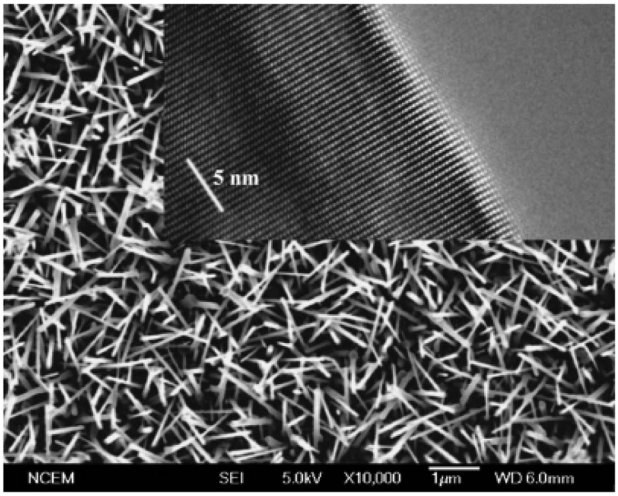

ZnO nanowires formed by fs-laser-assisted growth with an inset showing the side of a nanowire with TEM. Reprinted with permission from Y. Zhang *et al.*, Appl. Phys. Lett. **87**, 133115 (2005) [120]. Copyright 2005, AIP Publishing LLC.

with PLD [59]. There is an especially large amount of activity in using PLD to test a variety of up-and-coming higher mobility p-type transparent conductive oxide materials for thin-film photovoltaic and transistor applications [117]. Repeating these results at larger scale in a low-cost photovoltaic industrial setting is unlikely, however, due to the low throughput and nanoparticle ejection problems associated with PLD [117,118].

4.3c. Laser-Assisted Growth

The use of lasers to help start nanowire growth is a relatively new field and has been applied to a variety of semiconductors. Nanowire growth was first discovered using a ns laser acting on a $Si_{1-x}Fe_x$ target, where the researchers found a large size distribution of the resulting nanowires [119]. The growth mechanism proposed that the formation of the nanowires occurs while the ablated nanoclusters are still in the liquid phase and that the length of the nanowire growth is determined by the time that it takes for the nanowire to be pushed out of the "hot reaction zone" by the flowing carrier gas in the chamber [119]. The nanowires created consist of a single crystalline Si core with a SiO_x sheath on the outside and are on the order of tens of nanometers. It has also been shown that it is possible to extend this method to other materials, such as germanium (Ge), but unlike the Si nanowires, the Ge nanowires tend to have no amorphous outer shell and have a nanocluster at the termination end, showing that nanowire formation is a complicated procedure and is still not completely understood for all materials.

By moving to fs lasers, researchers found that it was possible to apply this process to oxides. Using a zinc oxide (ZnO) target, the researchers showed that it was possible to control the size distribution of the nanowires due to the lack of overall thermal effects and smaller particulate creation with the nanoparticles flying off of the target. They were also able to control the photoluminescence properties by changing the ambient oxygen partial pressure parameters [120]. They used a ZnO target and focused the laser inside the growth chamber with oxygen flowing. By using a fs laser instead of the ns laser used prior, there is no real melting in the ablation process, and they use Coulomb explosion to produce precise nanowires that have a small size distribution. With the fs lasers, there is less particulate formation, leading to a superior nanowire product [120]. The nanowires are shown with a transmission electron microscopy (TEM) inset showing their crystallinity in Fig. 14 [120]. By applying these methods to other materials, it should be possible to grow various materials and control their size and makeup.

5. CONCLUSION

In this paper, we present the various applications of ultrafast (fs–ns time regime) laser processing of various materials, specifically semiconductors. We show that the fs laser leads to finer structure formation and more precise machining when compared to the ns-laser regime, which can be utilized in a variety of applications. Thermal and nonthermal processes need to be balanced to control the microstructural features. In addition, we show that ultrafast lasers can be used as the basis for a few deposition techniques. With advances in how fs lasers operate, we believe that they will be used even more in the coming years as the applications become more diverse and the lasers become smaller and more cost-effective.

ACKNOWLEDGMENTS

Several people contributed to the work described in this paper. K. P. and H. G. prepared the manuscript. E. M. and S. K. S. supervised the work. The authors thank Ben Franta and Alex Raymond for editing the manuscript. K. P. and H. G.

acknowledge support from the National Science Foundation Graduate Research Fellowship under Grant Nos. DGE 0644491 and DGE 0946799 and the Department of Defense (DoD) through the National Defense Science and Engineering Graduate Fellowship (NDSEG) Program. E. M. acknowledges a vested interest in SiOnyx, Inc. S. K. S. acknowledges support from the Kyocera Corporation in the form of Inamori Professorship at The New York College of Ceramics at Alfred University.

REFERENCES

1. R. Kienberger, X. Chang, and C. H. Nam, "10th anniversary of attosecond pulses," J. Phys. B **45**, 070201 (2012).
2. B. Gu, "Ultrafast laser applications in semiconductor industry," Proc. SPIE **5339**, 226–230 (2004).
3. K. Sugioka and Y. Cheng, "Ultrafast lasers—reliable tools for advanced materials processing," Light Sci. Appl. **3**, e149 (2014).
4. D. Bastings, K. Pippert, and U. Stamm, "History and future prospects of excimer laser technology," in *Riken Focused on 2nd International Symposium on Laser Precision Microfabrication (LPM 2001)*, Lambda Physik AG, Germany, January 2002.
5. M. DiDomenico, "Small-signal analysis of internal (coupling-type) modulation of lasers," J. Appl. Phys. **35**, 2870 (1964).
6. L. E. Hargrove, R. L. Fork, and M. A. Pollack, "Locking of He-Ne laser modes induced by synchronous intracavity modulation," Appl. Phys. Lett. **5**, 4 (1964).
7. P. Maine, D. Strickland, P. Bado, M. Pessot, and G. Mourou, "Generation of ultrahigh peak power pulses by chirped pulse amplification," IEEE J. Quantum Electron. **24**, 398–403 (1988).
8. C. E. Cook, "Pulse compression-key to more efficient radar transmission," Proc. IRE **48**, 310–316 (1960).
9. M. Perry, "Multilayer dielectric gratings: increasing the power of light," Sci. Technol. Rev. 24–33 (1995).
10. D. Strickland and G. Mourou, "Compression of amplified chirped optical pulses," Opt. Commun. **55**, 447–449 (1985).
11. M. Pessot, P. Maine, and G. Mourou, "1000 times expansion/compression of optical pulses for chirped pulse amplification," Opt. Commun. **62**, 419–421 (1987).
12. S. Zhou, L. Kuznetsova, A. Chong, and F. Wise, "Compensation of nonlinear phase shifts with third-order dispersion in short-pulse fiber amplifiers," Opt. Express **13**, 4869–4877 (2005).
13. L. Kuznetsova and F. W. Wise, "Scaling of femtosecond Yb-doped fiber amplifiers to tens of microjoule pulse energy via non linear pulse amplification," Opt. Lett. **32**, 2671–2673 (2007).
14. M. E. Fermann and I. Hartl, "Ultrafast fibre lasers," Nat. Photonics **7**, 868–874 (2013).
15. S. K. Sundaram and E. Mazur, "Inducing and probing non-thermal transitions in semiconductors using femtosecond laser pulses," Nat. Mater. **1**, 217–224 (2002).
16. M. T. Winkler, "Non-equilibrium chalcogen concentrations in silicon: physical structure, electronic transport, and photovoltaic potential," Ph.D. thesis (Harvard University, 2009).
17. C. Dorman, "Picosecond micromachining update unique fiber-based laser technology delivers high pulse energy and average power," Laser Tech. J. **5**, 44–47 (2008).
18. J. M. Liu, R. Yen, H. Kurz, and N. Bloembergen, "Phase transformation on and charged particle emission from a silicon crystal surface, induced by picosecond laser pulses," Appl. Phys. Lett. **39**, 755–757 (1981).

19. J. M. Liu, H. Kurz, and N. Bloembergen, "Picosecond time-resolved plasma and temperature-induced changes of reflectivity and transmission in silicon," Appl. Phys. Lett. **41**, 643–646 (1982).
20. D. von der Linde and N. Fabricius, "Observation of an electronic plasma in picosecond laser annealing of silicon," Appl. Phys. Lett. **41**, 991–993 (1982).
21. J. A. Kittl, P. G. Sanders, M. J. Aziz, D. P. Brunco, and M. O. Thompson, "Complete experimental test of kinetic models for rapid alloy solidification," Acta Mater. **48**, 4797–4811 (2000).
22. B. N. Chichkov, C. Momma, S. Nolte, F. von Alvensleben, A. Tunnermann, F. Alvensleben, and A. Tünnermann, "Femtosecond, picosecond and nanosecond laser ablation of solids," Appl. Phys. A **63**, 109–115 (1996).
23. P. Lorazo, L. J. Lewis, and M. Meunier, "Thermodynamic pathways to melting, ablation, and solidification in absorbing solids under pulsed laser irradiation," Phys. Rev. B **73**, 134108 (2006).
24. J. E. Sipe, J. F. Young, J. S. Preston, and H. M. Vandriel, "Laser-induced periodic surface structure. I. Theory," Phys. Rev. B **27**, 1141–1154 (1983).
25. B. R. Tull, J. E. Carey, E. Mazur, J. P. McDonald, and S. M. Yalisove, "Silicon surface morphologies after femtosecond laser irradiation," MRS Bull. **31**, 626–633 (2006).
26. J. Bonse and J. Kruger, "Pulse number dependence of laser-induced periodic surface structures for femtosecond laser irradiation of silicon," J. Appl. Phys. **108**, 034903 (2010).
27. J. F. Young, J. E. Sipe, and H. M. Vandriel, "Laser-induced periodic surface structure. III. Fluence regimes, the role of feedback, and details of the induced topography in germanium," Phys. Rev. B **30**, 2001–2015 (1984).
28. H. van Driel, J. Sipe, and J. Young, "Laser-induced periodic surface structure on solids: a universal phenomenon," Phys. Rev. Lett. **49**, 1955–1958 (1982).
29. T. J.-Y. Derrien, R. Koter, J. Kruger, S. Hohm, A. Resenfeld, and J. Bonse, "Plasmonic formation mechanism of periodic 100-nm-structures upon femtosecond laser irradiation of silicon in water," J. Appl. Phys. **116**, 074902 (2014).
30. T. J.-Y. Derrien, T. E. Itna, R. Torres, T. Sarnet, and M. Sentis, "Possible surface plasmon polariton excitation under femtosecond laser irradiation of silicon," J. Appl. Phys. **114**, 083104 (2013).
31. G. Dumitru, V. Romano, H. P. Weber, M. Sentis, and W. Marine, "Femtosecond ablation of ultrahard materials," Appl. Phys. A **74**, 729–739 (2002).
32. J. Reif, O. Varalamova, and F. Constache, "Femtosecond laser induced nanostructure formation: self-organization control parameters," Appl. Phys. A **92**, 1019–1024 (2008).
33. J. Reif, F. Costache, O. Varlamova, G. Jia, and M. Tatzke, "Self-organized regular surface patterning by pulsed laser ablation," Phys. Status Solidi **6**, 681–686 (2009).
34. J. Reif, O. Varlamova, S. Uhlig, S. Varlamov, and M. Bestehorn, "On the physics of self-organized nanostructure formation upon femtosecond laser ablation," Appl. Phys. A **117**, 179–184 (2014).
35. Clark-MXR Inc., "Machining with ultrafast pulses," 2011, http://www.cmxr.com/Education/Short.html.
36. N. Sudani, "Thin wafer dicing using a high repetition rate femtosecond laser," Master's thesis (Ryerson University, 2009).
37. Clark-MXR Inc., "Machining with long pulse lasers," 2011, http://www.cmxr.com/Education/Long.html.
38. C. B. Moore, *Chemical and Biochemical Applications of Lasers* (Elsevier, 2012), Vol. **1**.

39. A. Sabbah and D. Riffe, "Femtosecond pump-probe reflectivity study of silicon carrier dynamics," Phys. Rev. B **66**, 165217 (2002).
40. P. Saeta, J.-K. Wang, Y. Siegal, N. Bloembergen, and E. Mazur, "Ultrafast electronic disordering during femtosecond laser melting of GaAs," Phys. Rev. Lett. **67**, 1023–1026 (1991).
41. Y. Dikmelik, C. McEnnis, and J. B. Spicer, "Femtosecond and nanosecond laser-induced breakdown spectroscopy of trinitrotoluene," Opt. Express **16**, 5332 (2008).
42. R. R. Frontiera, A.-I. Henry, N. L. Gruenke, and R. P. Van Duyne, "Surface-enhanced femtosecond stimulated Raman spectroscopy," J. Phys. Chem. Lett. **2**, 1199–1203 (2011).
43. B. K. Nayak, V. V. Iyengar, and M. C. Gupta, "Efficient light trapping in silicon solar cells by ultrafast-laser-induced self-assembled micro/nano structures," Prog. Photovoltaics **19**, 631–639 (2011).
44. T. Jia, H. Chen, M. Huang, F. Zhao, J. Qiu, R. Li, Z. Xu, X. He, J. Zhang, and H. Kuroda, "Formation of nanogratings on the surface of a ZnSe crystal irradiated by femtosecond laser pulses," Phys. Rev. B **72**, 125429 (2005).
45. K. Okamuro, M. Hashida, Y. Miyasaka, Y. Ikuta, S. Tokita, and S. Sakabe, "Laser fluence dependence of periodic grating structures formed on metal surfaces under femtosecond laser pulse irradiation," Phys. Rev. B **82**, 1–5 (2010).
46. S. K. Das, K. Dasari, A. Rosenfeld, and R. Grunwald, "Extended-area nanostructuring of TiO_2 with femtosecond laser pulses at 400 nm using a line focus," Nanotechnology **21**, 155302 (2010).
47. E. C. Landis, K. C. Phillips, E. Mazur, and C. M. Friend, "Formation of nanostructured TiO_2 by femtosecond laser irradiation of titanium in O_2," J. Appl. Phys. **112**, 063108 (2012).
48. V. V. Iyengar, B. K. Nayak, and M. C. Gupta, "Optical properties of silicon light trapping structures for photovoltaics," Solar Energy Mater. Solar Cells **94**, 2251–2257 (2010).
49. M.-J. Sher, M. T. Winkler, and E. Mazur, "Pulsed-laser hyperdoping and surface texturing for photovoltaics," MRS Bull. **36**, 439–445 (2011).
50. C. H. Crouch, J. E. Carey, J. M. Warrender, M. J. Aziz, E. Mazur, and F. Y. Genin, "Comparison of structure and properties of femtosecond and nanosecond laser-structured silicon," Appl. Phys. Lett. **84**, 1850–1852 (2004).
51. V. V. Iyengar, B. K. Nayak, K. L. More, H. M. Meyer, M. D. Biegalski, J. V. Li, and M. C. Gupta, "Properties of ultrafast laser textured silicon for photovoltaics," Solar Energy Mater. Solar Cells **95**, 2745–2751 (2011).
52. B. G. Lee, L. Yu-Ting, S. Meng-Ju, E. Mazur, H. M. Branz, Y.-T. Lin, and M.-J. Sher, "Light trapping for thin silicon solar cells by femtosecond laser texturing," in *38th IEEE Photovoltaic Specialists Conference (PVSC)* (IEEE, 2012), pp. 1606–1608.
53. E. Yablonovitch and G. D. Cody, "Intensity enhancement in textured optical sheets for solar cells," IEEE Trans. Electron Devices **29**, 300–305 (1982).
54. V. Zorba, L. Persano, D. Pisignano, A. Athanassiou, E. Stratakis, R. Cingolani, P. Tzanetakis, and C. Fotakis, "Making silicon hydrophobic: wettability control by two-lengthscale simultaneous patterning with femtosecond laser irradiation," Nanotechnology **17**, 3234–3238 (2006).
55. T. Baldacchini, J. E. Carey, M. Zhou, and E. Mazur, "Superhydrophobic surfaces prepared by microstructuring of silicon using a femtosecond laser," Langmuir **22**, 4917–4919 (2006).
56. R. Buividas, M. Mikutis, T. Kudrius, A. Greičius, G. Šlekys, and S. Juodkazis, "Femtosecond laser processing—a new enabling technology," Lith. J. Phys. **52**, 301–311 (2012).

57. H. Wang, "Laser surface texturing, crystallization and scribing of thin films in solar cell applications," Ph.D. thesis (Columbia University, 2013).
58. H. Booth, "Laser processing in industrial solar module manufacturing," J. Laser Micro/Nanoeng. **5**, 183–191 (2010).
59. R. Bartlome, B. Strahm, Y. Sinquin, A. Feltrin, and C. Ballif, "Laser applications in thin-film photovoltaics," Appl. Phys. B **100**, 427–436 (2010).
60. P. Gecys, "Scribing of thin-film solar cells with picosecond and femtosecond lasers," J. Laser Micro/Nanoeng. **7**, 33–37 (2012).
61. D. Ruthe, K. Zimmer, and T. Höche, "Etching of $CuInSe_2$ thin films—comparison of femtosecond and picosecond laser ablation," Appl. Surf. Sci. **247**, 447–452 (2005).
62. T.-W. Kim, J.-Y. Lee, D.-H. Kim, and H.-J. Pahk, "Ultra-short laser patterning of thin-film CIGS solar cells through glass substrate," Int. J. Precis. Eng. **14**, 1287–1292 (2013).
63. A. Risch and R. Hellmann, "Picosecond laser patterning of ITO thin films," Phys. Procedia **12**, 133–140 (2011).
64. R. Patel, "Beam profile effect for thin film solar cell scribing," 2010, http://www.industrial-lasers.com/articles/print/volume-250/issue-6/features/beam-profile-effect-for-thin-film-solar-cell-scribing.html.
65. Rofin Lasertech GmbH, "Laser edge isolation," 2015, http://www.rofin.com/en/markets/photovoltaic-industry/laser-edge-isolation/.
66. F. Colville, "Laser scribing tools edge in front," Global Solar Technol. **2**, 12–15 (2009).
67. X. Sedao, T. Sarnet, M. Fares, M. Schlutz-Ruhtenberg, J. L. Hernandez, S. Krantz, and R. Russel, "High throughput laser junction isolation for silicon solar cells," in *25th European Photovoltaic Solar Energy Conference and Exhibition/5th World Conference on Photovoltaic Energy Conversion*, Valencia, Spain, 6–10 September 2010, pp. 2325–2328.
68. X. Sedao, T. Sarnet, J. L. Hernandez, M. Schlutz-Ruhtenberg, and S. Krantz, "Edge isolation using ultra-short pulse laser materials with a top hat beam profile," Adv. Mater. Res. **321**, 234–239 (2011).
69. O. Haupt, V. Schutz, and R. King, "Improved laser edge isolation of crystalline silicon solar cells using a high power picosecond laser," in *28th International Congress on Applications of Lasers and Electro-Optics*, Orlando, Florida, November 2–5, 2009, paper M 903.
70. V. Schütz, O. Haupt, U. Stute, H. Nagel, and G. Lorenz, "Laser edge isolation with focus on damage reduction by the use of ultra-short pulse lasers," in *25th European Photovoltaic Solar Energy Conference and Exhibition/5th World Conference on Photovoltaic Energy Conversion*, Valencia, Spain, September 6–10, 2010, pp. 1984–1990.
71. J. Bonse, M. Geuss, S. Baudach, H. Sturm, and W. Kautek, "The precision of the femtosecond-pulse laser ablation of TiN films on silicon," Appl. Phys. A **69**, S399–S402 (1999).
72. G. Kamlage, T. Bauer, A. Ostendorf, and B. N. Chichkov, "Deep drilling of metals by femtosecond laser pulses," Appl. Phys. A **77**, 307–311 (2003).
73. F. Korte, S. Nolte, B. N. Chichkov, T. Bauer, G. Kamlage, T. Wagner, C. Fallnich, and H. Welling, "Far-field and near-field material processing with femtosecond laser pulses," Appl. Phys. A **69**, S7–S11 (1999).
74. Z. W. H. Y. Zheng and X. C. Wang, "Laser dicing of silicon and electronic substrates," in *Advances in Laser Materials Processing: Technology, Research, and Application*, J. R. Lawrence, J. Pou, D. K. Y. Low, and E. Toyserkani, eds. (Woodhead, 2010), pp. 88–130.

75. J. S. Dahm, "Short pulsewidth, high pulse repetition frequency laser system," U.S. patent 5,870,421 (December 8, 1998).
76. A. Yokotani, T. Mukumoto, T. Mizuno, K. Kurosawa, K. Kawahara, T. Ninomiya, and H. Sawada, "Development of dicing technique for thin semiconductor substrates with femtosecond laser ablation," Proc. SPIE **4637**, 374–381 (2004).
77. J. Sillanpaa, J. Kangastupa, A. Salokatve, and H. Asonen, "Ultra short pulse laser meeting the requirements for high speed and high quality dicing of low-K wafers," in *IEEE/SEMI Advanced Semiconductor Manufacturing Conference and Workshop* (IEEE, 2005), pp. 194–196.
78. H. Tonshoff, A. Ostendorf, K. Korber, and N. Barsch, "Speed rate improvement for microcutting of thin silicon with femtosecond laser pulses," Proc. SPIE **4830**, 219–225 (2004).
79. C. Wu, C. H. Crouch, L. Zhao, J. E. Carey, R. Younkin, J. A. Levinson, E. Mazur, R. M. Farrell, P. Gothoskar, and A. Karger, "Near-unity below-band-gap absorption by microstructured silicon," Appl. Phys. Lett. **78**, 1850–1852 (2001).
80. D. Recht, "Energetic beam processing of silicon to engineer optoelectronically active defects," PhD. thesis (Harvard University, 2013).
81. M. T. Winkler, D. Recht, M.-J. Sher, A. J. Said, E. Mazur, and M. J. Aziz, "Insulator-to-metal transition in sulfur-doped silicon," Phys. Rev. Lett. **106**, 178701 (2011).
82. C. H. Crouch, J. E. Carey, M. Shen, E. Mazur, and F. Y. Genin, "Infrared absorption by sulfur-doped silicon formed by femtosecond laser irradiation," Appl. Phys. A **79**, 1635–1641 (2004).
83. M. A. Sheehy, B. R. Tull, C. M. Friend, and E. Mazur, "Chalcogen doping of silicon via intense femtosecond-laser irradiation," Mater. Sci. Eng. B **137**, 289–294 (2007).
84. B. R. Tull and E. Mazur, "Femtosecond laser ablation of silicon: nanoparticles, doping and photovoltaics," Ph.D. thesis (Harvard University, 2007).
85. M.-J. Sher, *Femtosecond Laser Textured and Hyperdoped Black Silicon* (Mazur Group, 2013).
86. R. Reitano, P. M. Smith, and M. J. Aziz, "Solute trapping of group-III, IV, and V elements in silicon by an aperiodic stepwise growth-mechanism," J. Appl. Phys. **76**, 1518–1529 (1994).
87. P. H. Bucksbaum and J. Bokor, "Rapid melting and regrowth velocities in silicon heated by ultraviolet picosecond laser-pulses," Phys. Rev. Lett. **53**, 182–185 (1984).
88. N. F. Mott and W. D. Twose, "The theory of impurity conduction," Adv. Phys. **10**, 107–163 (1961).
89. J. P. Mailoa, A. J. Akey, C. B. Simmons, D. Hutchinson, J. Mathews, J. T. Sullivan, D. Recht, M. T. Winkler, J. S. Williams, J. M. Warrender, P. D. Persans, M. J. Aziz, and T. Buonassisi, "Room-temperature sub-band gap optoelectronic response of hyperdoped silicon," Nat. Commun. **5**, 3011 (2014).
90. Z. H. Huang, J. E. Carey, M. G. Liu, X. Y. Guo, E. Mazur, and J. C. Campbell, "Microstructured silicon photodetector," Appl. Phys. Lett. **89**, 033506 (2006).
91. J. E. Carey, X. Li, and N. J. McCaffrey, "High sensitivity photodetectors, imaging arrays, and high efficiency photovoltaic devices produced using ion implantation and femtosecond laser irradiation," U.S. patent 8,679,959 (March 25, 2014).
92. K. C. Phillips, "Femtosecond laser processing of wide bandgap semiconductors and their applications," PhD. thesis (Harvard University, 2014).
93. J. M. P. Almeida, V. Tribuzi, R. D. Fonseca, A. J. G. Otuka, P. H. D. Ferreira, V. R. Mastelaro, P. Brajato, A. C. Hernandes, A. Dev, T. Voss, D. S. Correa, and

C. R. Mendonca, "Femtosecond laser processing of glassy and polymeric matrices containing metals and semiconductor nanostructures," Opt. Mater. **35**, 2643–2648 (2013).
94. A. Schneider, K. Sebald, A. Dev, K. Frank, A. Rosenauer, and T. Voss, "Towards optical hyperdoping of binary oxide semiconductors," J. Appl. Phys. **113**, 143512 (2013).
95. B. Eggleston, S. Varlamov, and M. Green, "Large-area diode laser defect annealing of polycrystalline silicon solar cells," IEEE Trans. Electron Devices **59**, 2838–2841 (2012).
96. W. Skorupa and H. Schmidt, *Subsecond Annealing of Advanced Materials – Annealing by Lasers, Flash Lamps, and Swift Heavy Irons*, Springer Series in Material Science (Springer, 2014), Vol. **192**.
97. B. K. Nayak and M. C. Gupta, "Femtosecond-laser-induced-crystallization and simultaneous formation of light trapping microstructures in thin a-Si:H films," Appl. Phys. A **89**, 663–666 (2007).
98. H. Wang, P. Kongsuwan, G. Satoh, and Y. L. Yao, "Femtosecond laser-induced simultaneous surface texturing and crystallization of a-Si:H thin film: morphology study," Int. J. Adv. Manuf. Technol. **65**, 1691–1703 (2012).
99. I. Theodorakos, I. Zergioti, V. Vamvakas, D. Tsoukalas, and Y. S. Raptis, "Picosecond and nanosecond laser annealing and simulation of amorphous silicon thin films for solar cell applications," J. Appl. Phys. **115**, 043108 (2014).
100. N. H. Rizvi, "Femtosecond laser micromachining: current status and applications," RIKEN Rev. **50**, 107–112 (2003).
101. R. R. Gattass and E. Mazur, "Femtosecond laser micromachining in transparent materials," Nat. Photonics **2**, 219–225 (2008).
102. D. Du, X. Liu, G. Korn, J. Squier, and G. Mourou, "Laser-induced breakdown by impact ionization in SiO_2 with pulse widths from 7 ns to 150 fs," Appl. Phys. Lett. **64**, 3071 (1994).
103. K. Sugioka, Y. Hanada, and K. Midorikawa, "Three-dimensional femtosecond laser micromachining of photosensitive glass for biomicrochips," Laser Photon. Rev. **4**, 386–400 (2010).
104. K. Sugioka, J. Xu, D. Wu, Y. Hanada, Z. Wang, Y. Cheng, and K. Midorikawa, "Femtosecond laser 3D micromachining: a powerful tool for the fabrication of microfluidic, optofluidic, and electrofluidic devices based on glass," Lab Chip **14**, 3447–3458 (2014).
105. S. Passinger, M. S. M. Saifullah, C. Reinhardt, K. R. V. Subramanian, B. N. Chichkov, and M. E. Welland, "Direct 3D patterning of TiO_2 using femtosecond laser pulses," Adv. Mater. **19**, 1218–1221 (2007).
106. M. S. Amer, M. A. El-Ashry, L. R. Dosser, K. E. Hix, J. F. Maguire, and B. Irwin, "Femtosecond versus nanosecond laser machining: comparison of induced stresses and structural changes in silicon wafers," Appl. Surf. Sci. **242**, 162–167 (2005).
107. D. J. Shir, E. C. Nelson, D. Chanda, A. Brzenski, P. V. Braun, J. A. Rogers, and P. Wiltzius, "Dual exposure, two-photon, conformal phase mask lithography for three dimensional silicon inverse woodpile photonic crystals," J. Vac. Sci. Technol. **28**, 783–789 (2010).
108. I. Mirza, G. O'Connell, J. J. Wang, and J. G. Lunney, "Comparison of nanosecond and femtosecond pulsed laser deposition of silver nanoparticle films," Nanotechnology **25**, 265301 (2014).
109. S. Amoruso, G. Ausanio, R. Bruzzese, M. Vitiello, and X. Wang, "Femtosecond laser pulse irradiation of solid targets as a general route to nanoparticle formation in a vacuum," Phys. Rev. B **71**, 033406 (2005).

110. S. Eliezer, N. Eliaz, E. Grossman, D. Fisher, I. Gouzman, Z. Henis, S. Pecker, Y. Horovitz, M. Fraenkel, S. Maman, and Y. Lereah, "Synthesis of nanoparticles with femtosecond laser pulses," Phys. Rev. B **69**, 144119 (2004).
111. S. Amoruso, R. Bruzzese, N. Spinelli, R. Velotta, M. Vitiello, X. Wang, G. Ausanio, V. Iannotti, and L. Lanotte, "Generation of silicon nanoparticles via femtosecond laser ablation in vacuum," Appl. Phys. Lett. **84**, 4502 (2004).
112. B. R. R. Tull, J. E. E. Carey, M. A. A. Sheehy, C. Friend, and E. Mazur, "Formation of silicon nanoparticles and web-like aggregates by femtosecond laser ablation in a background gas," Appl. Phys. A **83**, 341–346 (2006).
113. A. Kabashin, P. Delaporte, A. Pereira, D. Grojo, R. Torres, T. Sarnet, and M. Sentis, "Nanofabrication with pulsed lasers," Nanoscale Res. Lett. **5**, 454–463 (2010).
114. G. K. Hubler, "Pulsed laser deposition," MRS Bull. **17**, 26–29 (1992).
115. J. E. Dominguez, X. Q. Pan, L. Fu, P. A. Van Rompay, Z. Zhang, J. A. Nees, and P. P. Pronko, "Epitaxial SnO_2 thin films grown on $(\bar{1}012)$ sapphire by femtosecond pulsed laser deposition," J. Appl. Phys. **91**, 1060 (2002).
116. X. L. Tong, D. S. Jiang, W. B. Hu, Z. M. Liu, and M. Z. Luo, "The comparison between CdS thin films grown on Si(111) substrate and quartz substrate by femtosecond pulsed laser deposition," Appl. Phys. A **84**, 143–148 (2006).
117. A. E. Delahoy and S. Guo, "Transparent conductive oxides for photovoltaics," in *Handbook of Photovoltaic Science and Engineering*, A. Luque and S. Hegedus, eds., 2nd ed. (Wiley, 2011), pp. 716–796.
118. K. Ellmer, "Past achievements and future challenges in the development of optically transparent electrodes," Nat. Photonics **6**, 809–817 (2012).
119. A. M. Morales, "A laser ablation method for the synthesis of crystalline semiconductor nanowires," Science **279**, 208–211 (1998).
120. Y. Zhang, R. E. Russo, and S. S. Mao, "Femtosecond laser assisted growth of ZnO nanowires," Appl. Phys. Lett. **87**, 133115 (2005).

Katherine C. Phillips received her Ph.D. in Applied Physics from Harvard University in 2015, under the supervision of Prof. Eric Mazur. Her thesis research focused on femtosecond laser hyperdoping of wide bandgap semiconductors for energy applications and was funded through National Science Foundation (NSF) and National Defense Science and Engineering Graduate (NDSEG) fellowships. Prior to Harvard, Katherine received her Master of Advanced Study in Mathematics from Cambridge University and her B.S. degrees in Physics and Mathematics from North Carolina State University, where she was a Park Scholar.

Hemi H. Gandhi is an Applied Physics doctoral student at Harvard University working under the supervision of Professor Eric Mazur. Hemi's research interests are focused on using pulsed lasers as fabrication tools for developing novel materials and manufacturing techniques for high performance optoelectronic devices. He is currently working on nanosecond and femtosecond laser processing to develop new materials for mid-infrared photodetectors and high-efficiency, low-cost photovoltaics. His graduate work is funded by the National Defense Science and Engineering Graduate (NDSEG) fellowship. Hemi studied physics and economics at Harvard College, where he was a National Toyota Community Scholar. While a Harvard undergrad, Hemi worked on

metamaterial fabrication in the Mazur group, founded the Harvard College Global Energy Initiative, and wrote for the editorial board of the *Harvard Crimson*. His opinion pieces have been widely covered by CNN *Money, The Huffington Post, USA Today*, and *The Harvard Political Review*.

Eric Mazur is the Balkanski Professor of Physics and Applied Physics at Harvard University, Dean of Applied Physics, and Vice President of the Optical Society. He is a prominent physicist known for his contributions in nanophotonics, an internationally recognized educational innovator, and a successful entrepreneur. In education he is widely known for his work on Peer Instruction, an interactive teaching method aimed at engaging students in the classroom and beyond. In 2014 Mazur became the inaugural recipient of the Minerva Prize for Advancements in Higher Education. He has received many awards for his work in physics and in education and has founded several successful companies. Mazur is Chief Academic Adviser for Turning Technologies, a company developing interactive response systems for the education market. Dr. Mazur has widely published in peer-reviewed journals and holds numerous patents. He has also written extensively on education and is the author of *Peer Instruction: A User's Manual* (Prentice Hall, 1997), a book that explains how to teach large lecture classes interactively, and of the *Principles and Practice of Physics* (Pearson, 2014), a book that presents a groundbreaking new approach to teaching introductory calculus-based physics. Mazur is a sought-after speaker on optics and on education.

S. K. Sundaram is an Inamori Professor of Materials Science and Engineering at the Kazuo Inamori School of Engineering, The New York State College of Ceramics at Alfred University, appointed in 2011. Prior to joining Alfred University, Dr. Sundaram began his research career in 1994 in the Pacific Northwest National Laboratory (PNNL), after earning his Ph.D. degree from the Georgia Institute of Technology, and became the Chief Materials Scientist at the lab in 2002. Dr. Sundaram's major areas of interest are terahertz/millimeter wave science and technology, ultrafast materials science and engineering multi-scale materials processing, and infrared materials and technologies. Dr. Sundaram is an elected Fellow of the American Association of Advancement of Sciences (2006), the American Ceramic Society (2006), and the Society of Glass Technology UK (2009), and a member of the Optical Society of America (OSA).